



Electrodeposition of SnSe thin film using an organophosphorus [(Me₂)₃N₃PSe] precursor for photovoltaic application

Amira Ben Hjal^{1,2} · Luca Pezzato² · Elena Colusso² · Khaled Alouani¹ · Manuele Dabalà²

Received: 27 June 2023 / Revised: 31 August 2023 / Accepted: 6 October 2023
© The Author(s) 2023

Abstract

One prevalent class of thin films concerns SnSe (tin selenide), which is the primary focus of this research, with the aim of discovering cost-effective coatings for photovoltaic applications. The electrodeposition method was employed to successfully synthesize tin selenide thin films on glass substrates (ITO and FTO) utilizing the novel organophosphorus precursor [(Me₂)₃N₃PSe]. Notably, this precursor has not been utilized in prior literature. Initial cyclic voltammetry (CV) analyses were performed to thoroughly investigate the electrochemical behavior of the tin and selenium redox systems within the electrolyte. The CV outcomes yielded crucial insights, guiding the establishment of a defined potential range (− 1.1 to − 1.2 V vs. SCE) for effective SnSe film electrodeposition. Films deposited within this potential range exhibited characteristic needle-shaped polycrystalline SnSe structures. Comprehensive analyses of the thin films' structural, microstructural, and morphological characteristics were conducted, employing X-ray diffraction (XRD), Raman spectroscopy, and scanning electron microscopy with energy-dispersive X-ray spectroscopy (SEM/EDS). The crystallites' size was determined using the Debye–Scherrer formula. Moreover, a systematic exploration of the impact of deposition potential and substrate type on various film properties was undertaken. The results from XRD and Raman spectroscopy confirmed the formation of an orthorhombic single-phase SnSe under different deposition potentials. SEM/EDS analysis revealed uniform element distribution for deposition potentials of − 1.1 V and − 1 V on ITO and FTO substrates, respectively. The investigation further extended to the optical properties of films on glass substrates (ITO and FTO). Optical data showed a direct optical band gap (E_g) ranging from 1.25 to 2.24 eV for ITO and 1.46 to 2.87 eV for FTO across a wide spectra range. These optical traits, significantly influenced by deposition potential and substrate type, hold promise. Particularly, SnSe thin films deposited on ITO substrates at − 1.1 V displayed distinct advantages for potential photovoltaic applications compared to samples on FTO substrates.

Keywords Thin film · SnSe · Precursor · Electrodeposition · Optical properties

Introduction

The baseline scenario presented by the International Energy Agency (IEA) predicts a 55% increase in global primary energy consumption between 2005 and 2030, primarily driven by the rapid growth of emerging countries [1]. This surge in demand, coupled with the depletion and escalating costs of fossil fuels (oil, gas, coal), which currently account

for 60% of the world's power generation, has prompted a shift toward renewable energy sources. In recent years, numerous governments have made significant efforts to develop these sustainable energy alternatives. Renewable energies, as defined by the Agency for the Environment and Energy Management (ADEME), are derived from natural mechanisms such as solar radiation, tides, and wind and offer the advantages of being inexhaustible and emission-free compared to fossil fuels. Among these renewable energy sources are wind energy, tidal energy, geothermal energy, and solar photovoltaic energy, which is the focus of this research. Solar power generation has experienced exponential growth in recent decades, driven by declining costs per kilowatt-hour (kWh), advancements in conversion efficiency, and reduced manufacturing expenses. Overcoming technical challenges in thin film deposition processes, for instance, is

✉ Luca Pezzato
luca.pezzato@unipd.it

¹ Laboratory of Analytical Chemistry and Electrochemistry, Faculty of Science, University of Tunis El Manar, Campus, 2092 Tunis, Tunisia

² Department of Industrial Engineering, University of Padova, Via Marzolo, 9-35131 Padua, Italy

a key area of focus for many researchers in the field. Among these, Perovskite solar cells (PSCs) emerge as a compelling alternative, distinguished by their exceptional light absorption characteristics and streamlined manufacturing processes [2–4]. However, prevailing thin film technologies in the market encounter challenges related to scalability and extended development cycles. This limitation is primarily attributed to their reliance on rare and costly materials, including indium and gallium (as evidenced in CIGS technology), as well as cadmium tellurium (as observed in CdTe technology).

To overcome these challenges, tin selenide (SnSe) emerges as a promising alternative. SnSe is composed of naturally abundant elements and possesses a band gap ranging from 1 to 1.1 eV [1, 5, 6]. Its unique optical and electrical properties make it an attractive candidate for various applications, including solar cells, photoconductors, holographic recording media, and near-infrared detectors [5, 7, 8]. Compared to widely studied materials like CdS and CdSe, SnSe is less toxic to the environment and more readily available in nature. Consequently, SnSe holds great potential as a photovoltaic material for photoelectrochemical applications.

Various methods have been employed to fabricate thin films, including chemical bath deposition (CBD) [9], vacuum evaporation [10], chemical vapor deposition (CVD) [11], thermal evaporation [12], the hydrothermal method [13], radio frequency (RF) sputtering [14], successive ionic layer adsorption and reaction (SILAR) [15], laser ablation [16], electrochemical atomic layer epitaxy (ECALE) [17], and electrodeposition [18–24]. Among these techniques, electrodeposition stands out due to several advantages [19]. Firstly, it enables the deposition of thin films on large-area substrates, including flexible materials such as plastics. Secondly, the thickness and composition of the films can be easily controlled by adjusting deposition parameters such as deposition potential, pH, temperature, and time. Lastly, electrodeposition is generally a cost-effective method in terms of equipment requirements. Various electrodeposition approaches have been documented, including pulse electrodeposition [20], underpotential deposition (UPD) [21], and cathodic electrodeposition [22]. This method has been successfully applied to obtain thin films of materials such as PbS [20], CdS [21], $\text{Bi}_2\text{Te}_{3-y}\text{Se}_y$ [25], and CdS nanowires [26]. In a separate study on semiconductor thin films, we recently reported the electrodeposition of $\text{Bi}_{1-x}\text{Sb}_x$ and $\text{Bi}_{2-x}\text{Sb}_x\text{Te}_3$ thin films under underpotential deposition (UPD) and overpotential deposition (OPD) conditions [27].

Therefore, this research aims to systematically investigate the influence of deposition potential on the structural and morphological properties of SnSe thin films electrodeposited on ITO and FTO glass substrates for potential application in photovoltaic cells. The electrodeposition of SnSe thin films is carried out at room temperature using

two different approaches: deposition from two separate precursors or simultaneous deposition of both elements from a single solution. Various selenium precursors have been employed in previous studies for synthesizing tin selenide, including SnCl_2 , Na_2SeO_3 , or $(\text{NH}_4)_2\text{SeO}_3$ from aqueous solutions [28], as well as more recent compounds containing an M-Se bond, such as $[\text{Bu}_2\text{M}(\text{PhCOSe})_2]$ [29] and $[\text{MCl}_3(\text{SenDu}_2)_3]$ [30] (M = metal). Despite their ability to produce high-quality thin films with interesting properties, most of these procedures suffer from the use or formation of volatile and toxic by-products. To address these limitations, one approach is to replace these compounds with more stable precursors [31, 32]. In this study, we employ the stable molecule dimethylamino-selenophosphoramidate $[(\text{Me}_2)_3\text{N}_3\text{PSe}]$, which can be transformed into the environmentally friendly compound $[(\text{Me}_2)_3\text{N}_3\text{P}]$ or used directly as the main precursor $[(\text{Me}_2)_3\text{N}_3\text{PSe}]$. It is worth noting that, to the best of our knowledge, no thin film material has been deposited using this compound via the electrodeposition method, making this work novel in its approach.

The novelty of this work lies in the utilization, for the first time, of a stable and non-toxic organophosphorus precursor. In this study, we investigated the electrochemical behaviors of Sn and Se through cyclic voltammetry, aiming to comprehend their deposition potentials. Our endeavor aimed to achieve stoichiometric thin films of SnSe, which is an ideal alloy for depositing tin and selenium onto ITO and FTO substrates. By employing a consistent deposition potential, our goal was to attain thin SnSe films with the desired composition. Furthermore, we delved into the impact of the deposition potential on the film composition, morphology, and its interactions with the substrate material.

Experimental

At room temperature, we conducted cyclic voltammetry and electrodeposition experiments using a GAMRY model 2273 potentiostat/galvanostat connected to a three-electrode cell. For optical measurements, we utilized a commercial indium tin oxide (ITO)-coated glass substrate and a fluorine-doped tin oxide (FTO)-coated glass substrate (Sigma-Aldrich). The reference electrode in all electrochemical experiments was a 3M NaCl Hg/Hg₂Cl₂ (SCE) electrode, and the counter electrode was a platinum electrode.

The solutions used in the experiments were prepared using deionized water, and they were purged with purified Ar gas prior to each experiment. The solutions were not stirred during the electrochemical measurements and deposition processes. The electrodeposition solution for SnSe thin films consisted of 20 mM SnCl_2 ($\text{SnCl}_2 \cdot 2\text{H}_2\text{O}$, Sigma-Aldrich), 5 mM $(\text{Me}_2)_3\text{N}_3\text{PSe}$ (synthesized by reacting dimethylamino-phosphine with selenium powder, confirmed by ¹H and ¹³P

NMR), and 0.2 M $\text{Na}_2\text{C}_2\text{O}_4$ (Sigma-Aldrich). The pH of the solution was adjusted to 2 using 37% HCl acid. The addition of $\text{Na}_2\text{C}_2\text{O}_4$ helped form a SnC_2O_4 complex, preventing the hydrolysis of SnCl_2 in the aqueous solution and the formation of $\text{Sn}(\text{OH})\text{Cl}$ precipitate [33]. The deposition potential for SnSe was determined based on cyclic voltammetry data for Sn and Se in the presence of $\text{Na}_2\text{C}_2\text{O}_4$, resulting in a range between -1 and -1.2 V. After each electrodeposition, the SnSe thin films were rinsed with deionized water and air-dried at room temperature.

To characterize the films, various techniques were employed. XRD patterns were collected using a glancing incidence X-ray diffractometer (Philips PW1710 diffractometer) with CuK_α radiation in the angular range of 20 to 70° and a 1° incidence angle. Raman spectrometry was performed using a Horiba Jobin Yvon LabRam HR 800 spectrometer with a 530-nm wavelength. The surface morphologies of the deposited films were examined using a LEICA LEO 440 scanning electron microscope (SEM), while the chemical composition was analyzed through EDS analysis using a Philips PV9800 EDS system. Reflectance spectra in the 400–2000 nm range were recorded using a VIS–NIR V770 Jasco spectrophotometer equipped with an integrating sphere (ISN-470).

Results and discussion

Electrochemical behavior of the components

Electrochemical stability window

The electrochemical behavior of the electrolyte carrier solution was investigated prior to electrodeposition (Fig. 1).

Linear sweep voltammograms for the bath containing only the virgin solution, acidified at pH 2 by HCl and without the addition of $\text{Na}_2\text{C}_2\text{O}_4$, show the reduction reaction of H^+ to H_2 (Eq. (1)) starting at -1.5 V on the FTO substrate and the beginning of solvent decomposition at -1.1 V on the ITO substrate. From 1.74 V on fluorine-doped tin oxide (FTO) and 1.40 V on indium-doped tin oxide (ITO), the oxidation reaction of H_2O to O_2 (Eq. (2)) is observed.



At the same pH, in the presence of oxalate salt, solvent decomposition occurs at lower overpotentials for the reduction and oxidation signals than in the absence of oxalate. The electrochemical stability window on FTO ranges from -1.1 to 0.92 V, and on ITO as a substrate, favoring the redox reactions of the electrolyte solution ranges from -1.1 to 0.44 V.

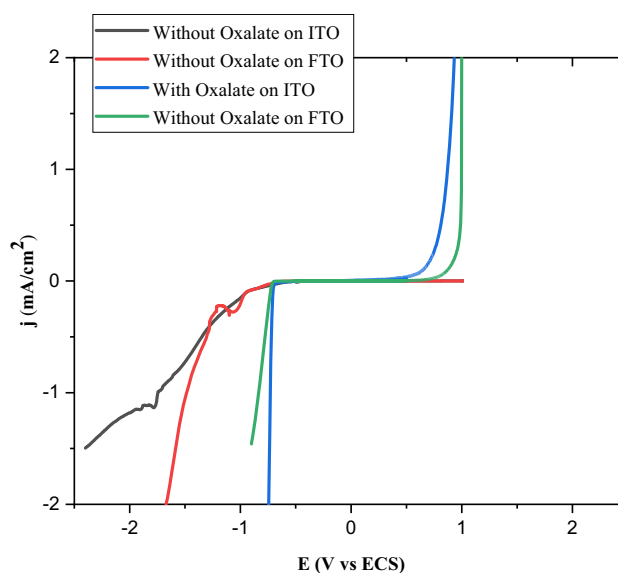


Fig. 1 Linear sweep voltammetry on the free Sn and Se electrolyte solution performed at room temperature with a scan rate of 10 mV.s^{-1}

Tin- and selenium-based systems

Tin-related systems To better understand the actual electrochemical system of SnSe, we first studied the individual behavior of Sn and Se in the bath. Figure 2a shows a reduction peak R_1 at -0.86 V (Eq. (3)) attributed to the reduction of Sn(II) to Sn(0) and a first oxidation peak $O1$ at -0.28 V corresponding to the anodic reaction.



At approximately 1.06 V, a broad and weak anodic peak labeled as O_2 is observed. This peak is associated with the oxidation of Sn(II) to Sn(IV), according to Eq. (4). The appearance of this signal can be attributed to the formation of SnO_2 .



At the same pH, CV was performed with and without oxalate in the solution (Fig. 2a). In the presence of oxalate salt, all peaks shift in the negative direction. This observation clearly shows that the Sn(II) cation is complex in the presence of oxalate salt (Eq. (5)).

A crossover consistently appears at a potential called E_{CO} when changing the direction of the potential sweep in the anodic direction. The apparent equilibrium potential of the Sn(II)-Sn(0)-metal-ion system in the electrolyte is associated with this crossover potential.

In Fig. 2a, an E_{CO} value of -0.48 V vs. SCE is recorded in the absence of oxalate salt, and this value should be compared to the standard redox potential of -0.32 V vs. SCE

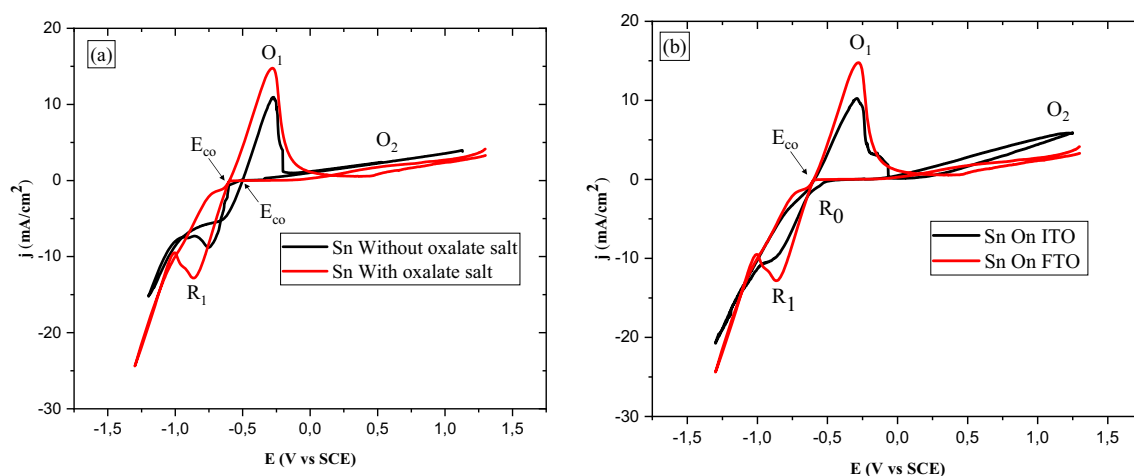
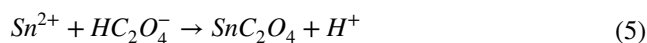
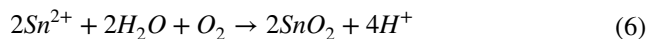


Fig. 2 Cyclic voltammety experiments on a 20-mM tin solution at $10 \text{ mV}\cdot\text{s}^{-1}$: (a) oxalate salt influence and (b) substrate influence

for $\text{Sn}^{2+}/\text{Sn}^0$ [34], the difference being due to cationic activity and possible complexation with chloride. Without and with oxalate salt, there is a cathodic shift of the E_{CO} value from -0.49 to -0.59 V. Based on literature data [35] and the acidic properties of oxalate, we propose the formation of a complex using the following equation:



This hypothesis is supported by the fact that in the absence of oxalate salt, the electrolyte solution remains turbid, likely due to the oxidation of tin by dissolved oxygen, resulting in the precipitation of SnO_2 (Eq. (6)).



The effect of the substrate is highlighted in Fig. 2b, which shows the comparative cyclic voltammety of the solution

using ITO and FTO as working electrodes. On ITO, the reduction peak R_1 has a lower absolute current density and is slightly shifted to -0.84 V rather than -0.86 V. Before the massive deposition (R_1 peak), an additional reduction peak R_0 can be observed at -0.56 V. This peak may correspond to underpotential deposition (UPD) of Sn(II) on the substrates, similar to the work of Mao et al. [36].

Selenium-related systems Cyclic voltammograms were acquired to evaluate the electrochemical behavior of the electrolyte containing our precursor, dimethylamino-selenophosphoramidate $(\text{Me}_2)_3\text{N}_3\text{PSe}$. This study was carried out with a scan rate of $10 \text{ mV}\cdot\text{s}^{-1}$ and a potential range of -1.5 to 1.5 V (vs. SCE). Figure 3 illustrates these results.

In this solution, the only electroactive species present is H_2SeO_3 , as selenium is released from the organophosphorus molecule in the form of Se(IV) in an acidic environment.

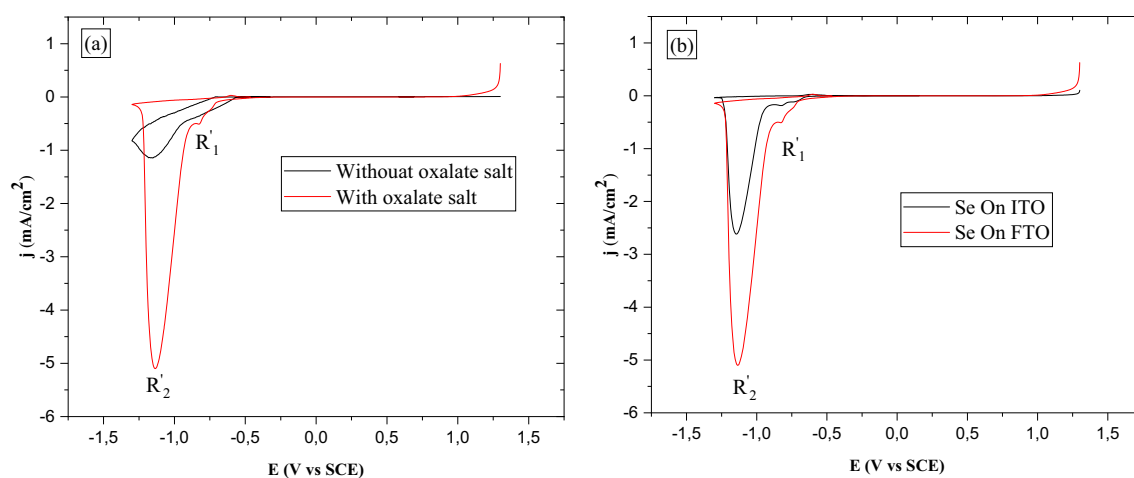
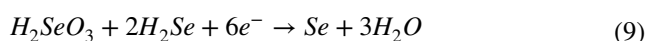
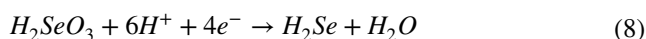
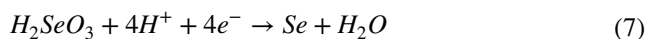


Fig. 3 Cyclic voltammety experiments on a 5-mM selenium solution at $10 \text{ mV}\cdot\text{s}^{-1}$: (a) oxalate salt influence and (b) substrate influence

When the oxalate salt is introduced into the solution, both reduction peaks show an increase in intensity. Cyclic voltammetry reveals a small cathodic peak labeled as R'_1 at -0.84 V, followed by a larger cathodic peak labeled as R'_2 at -1.11 V. The first peak R'_1 corresponds to the reduction of H_2SeO_3 to Se according to Eq. (7), although its size is too small to be clearly distinguished. The second peak R'_2 is likely associated with the reduction of H_2Se , according to Eq. (8). Following this reduction, H_2Se combines with dissolved H_2SeO_3 , as indicated by Eq. (9), leading to the formation of a red Se suspension. This phenomenon has been suggested by Massaccesi et al. [37] and Mishra [38].



By comparing the cyclic voltammograms of Figs. 2 and 3, it can be shown that Sn^{2+} and H_2SeO_3 were reduced in this order. Regardless of the chemical composition and type of working electrode, no anodic dissolution of Se^0 is observed.

According to the literature results, different and opposite electrochemical responses are observed depending on the working electrode. This results in the total absence of oxidation peaks on platinum or glassy carbon [39, 40]. On the other hand, Se is susceptible to undergo irreversible reduction, as seen, for example, on polycrystalline gold [41]. Based on the work of Ju et al. [37], we exclude the complexation of selenium by oxalate, which preferentially complexes tin. The fact that there is no visible cathodic change in the electrochemical behavior of Se with and without oxalate salt (Fig. 3a) is supportive of this hypothesis. However, in the absence of oxalate, the peaks are attenuated and unclear.

The cathodic peak intensities of R'_1 and R'_2 are higher on FTO than on ITO, as shown in Fig. 3b. According to Shi et al. [42], this observation could be due to the low electrochemical activity of the ITO substrate, resulting in low-intensity cyclic voltammetry curves.

These results indicate that the presence of oxalate in the electrolyte solution, as well as the use of ITO or FTO substrates at a bath temperature of $25^\circ C$, have a positive effect on the stability of the bath and the cathodic behavior of the simple elements Sn and Se. Therefore, these experimental parameters were selected to study the SnSe electrochemical system.

Tin selenide-related systems The electrolyte solution containing both Sn and Se, two electroactive species on ITO and FTO, was studied. Figure 4 shows cyclic voltammetry experiments performed at -1.5 V and 1.5 V (vs. SCE) and a

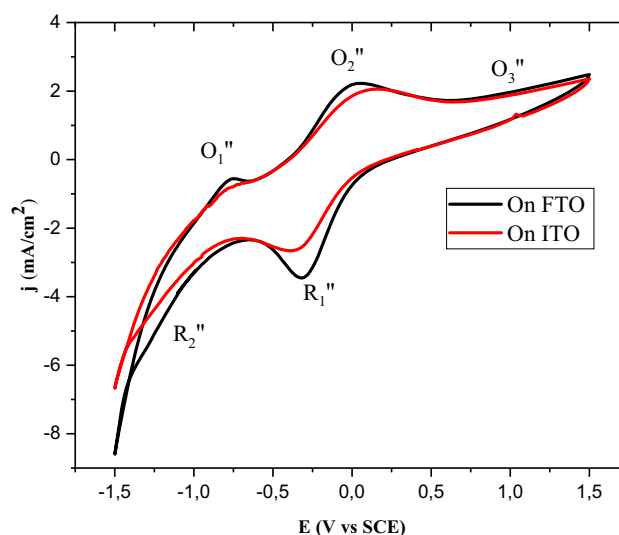


Fig. 4 Cyclic voltammetry experiments on a 20-mM tin and 5-mM selenium solution at $10 \text{ mV}\cdot\text{s}^{-1}$ on two distinct substrates (ITO and FTO)

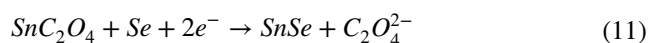
scan rate of 10 mV/s . A first reduction peak R''_1 is observed at -0.43 V, followed by a wide peak R''_2 starting from -1 V.

In the anodic scan, a small first oxidation peak O''_1 is noticed around -0.8 V, and two other oxidation peaks O''_2 and O''_3 are visible at -0.20 V and 1.1 V, respectively. These results allow us to deduce that R''_1 is related to O''_2 . Therefore, both R''_1 and O''_2 peaks can be confidently attributed to the tin metal system Sn^{2+}/Sn^0 according to Eq. (3). However, the attribution of the broad cathodic peak R''_2 is not straightforward. Compared to the individual behaviors of Sn and Se, the signal could be attributed to either Sn^0 UPD and/or bulk Se^0 deposition, respectively. Therefore, two options exist to produce SnSe in this potential range around R''_2 .

Firstly, as indicated by Ham et al. [43], we can study the reduction of Se(IV) to Se(-II) in the presence of Sn(II) (Eq. (10)). In other words, we can propose a mechanism in which the generation of SnSe involves the reduction of Se(IV) to Se(-II) without reduction of tin. The binary compound is then formed by the precipitation of SnSe.



The other alternative is a two-step deposition method, like the electrodeposition of SnSe thin films for photovoltaic applications [44]. The first step would be the reduction of Se(IV) to Se^0 according to Eq. (7), triggering the reduction of Sn(II), as shown in Eq. (11).



The deposition of SnSe is expected to occur in this potential range, regardless of the deposition process. However, fixed applied potential depositions were carried out to

gain a better understanding, and the results are discussed below. Based on cyclic voltammetry studies, the potential range of interest for SnSe film electrodeposition should be between -1 and -1.2 V.

Structural analysis

XRD analysis

To study the crystallinity of SnSe layers prepared by electrodeposition, we obtained XRD spectra on ITO and FTO at different potentials (-1 V, -1.1 V, -1.2 V) using a recorder, and the results are presented in Fig. 5.

In this Fig. 5, the peaks observed at $2\theta = 22.4, 26.38, 30.4, 30.8, 37.6, 40.4, 43.7, 44.8, 49.34, 61.39, 62.45, 63.69, 64.46,$ and 66.55 can be attributed to the crystal planes (101), (212), (111), (400), (401), (002), (020), (501), (511), (701), (512), (521), (711), and (322) that correspond to the orthorhombic phase of tin selenide with JCPDS map number 00-048-1224. The strongest diffraction peak (111) suggests a preferential growth direction regardless of the fixed potential applied and regardless of the nature of the working electrode (ITO or FTO). Weak diffraction peaks are detected for samples deposited on ITO and FTO at potentials of -1 V and -1.2 V, respectively, indicating that the optimal deposition potential for ITO is between -1.1 V and -1.2 V, while the best deposition potential for the FTO substrate is between -1 V and -1.1 V.

Using the Debye–Scherrer formula, we can determine the crystallite size of each plane [28]:

$$D = \frac{K\lambda}{\beta \cos\theta} \quad (12)$$

where K is a constant equal to 0.94, λ is the wavelength of the X-rays used, which is 1.54 Angstroms, β represents the full-width at half maximum (FWHM) of the peak, and θ is the diffraction angle.

The average crystallite size of the planes was 45.52 nm for ITO at -1.1 V and 34.14 nm for FTO at -1 V, which is an appropriate value in the case of electrical conduction. These results lead to the conclusion that the proposed process has allowed to production of an exceptional crystalline SnSe layer with high crystallite sizes and no impurity phase.

Raman spectroscopy analysis

Raman spectra (Fig. 6) were acquired for materials deposited at the same potentials between -1 V and -1.2 V on ITO and FTO to evaluate the likely presence of amorphous species or minor phases at concentrations too low to be identified by XRD.

The obtained Raman peaks are in good agreement with previous works [45]. According to group theory calculations, SnSe should have 12 Raman active modes: $4A_g, 2B_{1g}, 4B_{2g},$ and $2B_{3g}$. At a potential of -1.1 V, the expected SnSe Raman lines by group theory are at 117 cm^{-1} and 205 cm^{-1} in the A_g symmetry and at 165.71 cm^{-1} in the B_{3g} symmetry [29, 46, 47]. The Raman shift for thin films deposited at -1 V was not significant, with only vibrational modes at 117 cm^{-1} detected, and the others were difficult to assign due to the broadening of the peaks.

However, thin films formed at -1.2 V exhibited distinct peaks, with a strongly intense mode present at 117 cm^{-1} . The frequency and width change could be attributed to

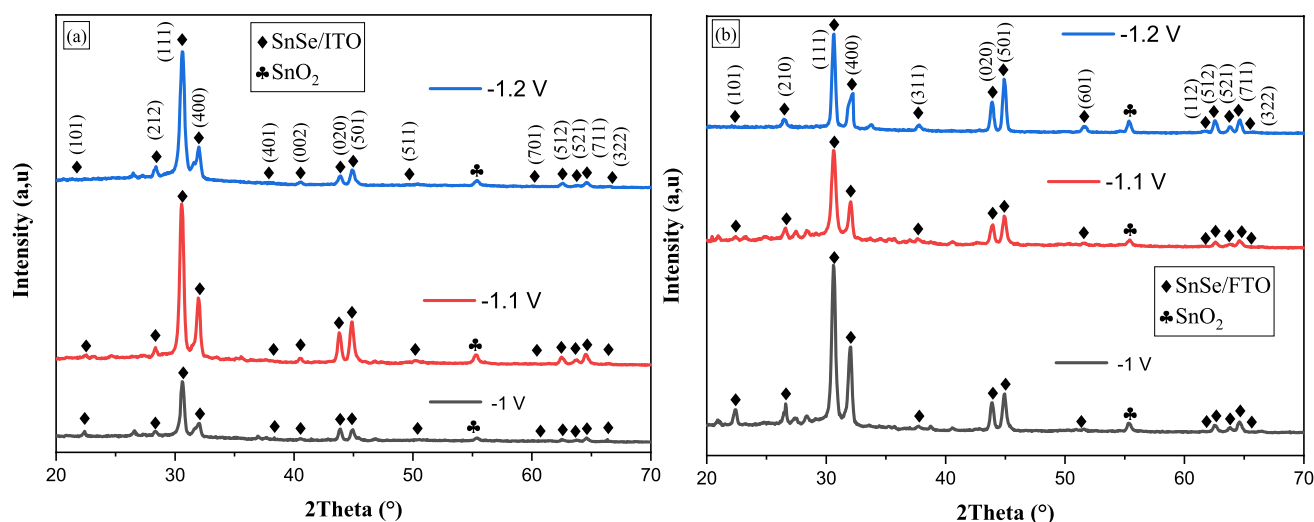


Fig. 5 XRD patterns of SnSe deposited at different potentials on (a) ITO and (b) FTO

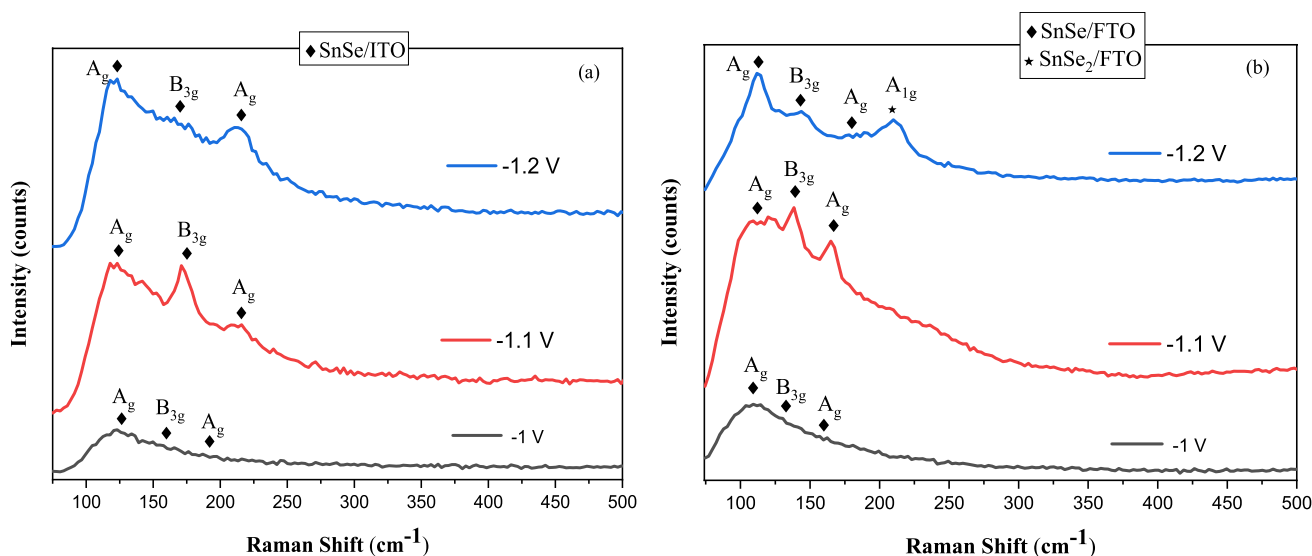


Fig. 6 Raman spectra for SnSe thin films deposited at different potentials on (a) ITO and (b) FTO

phonon softening and increased electron–phonon coupling in a thin film structure [48]. The bands became sharper and more intense, and the maximum intensity ratio was found for the thin film deposited at a potential of -1.1 V for the ITO substrate, demonstrating the superior structural quality of the film compared to other potentials.

The findings from the electrodeposition of SnSe thin films onto FTO (Fig. 6b) exhibit a strong resemblance to the ITO spectra (Fig. 6a). However, two bands, representative of SnSe, are observed at 115 cm^{-1} and 196 cm^{-1} . They are attributed to the two A_g vibrational modes of SnSe. Around 160 cm^{-1} , a strong band seems to be a B_{3g} vibrational mode [29]. Another mode, found at 213 cm^{-1} with a deposition potential of -1.2 V, is related to the A_{1g} vibrational mode of SnSe_2 [49].

The attribution of this peak confirms the XRD analysis hypothesis that the deposits are mainly composed of SnSe, especially in the critical potential range of $-1.1/-1.2$ V for the ITO working electrode, and in the potential range of $-1/-1.1$ V which is significant for the FTO electrode.

SEM and EDS analysis

Scanning electron microscopy (SEM) was used to examine the surface morphology of the films formed on ITO and FTO substrates, and the results are presented in Fig. 7, which displays typical surface images of the samples obtained for different fixed potentials ranging from -1 to -1.2 V. Depending on the applied potential, different microstructures are detected.

The application of a potential of -1 V on the ITO substrate results in uneven surface morphology of the layers, as shown in the SEM images of Fig. 7a. On the other hand,

for the other two potentials, -1.1 V and -1.2 V, the SEM images in Fig. 7a show several rectangular grains uniformly distributed on the surface of the SnSe thin film, as observed by Biçer et al. for films electrodeposited in the presence of EDTA [25] as well as for SnSe films prepared by electro-deposition on ITO [50, 51]. These results are consistent with those obtained from X-ray analysis and Raman spectroscopy, as shown in Figs. 5a and 6a, respectively, where the most intense preferential peak (111) was found between -1.1 and -1.2 V.

Based on the morphological characterization of the SnSe surface obtained by FTO electrodeposition (Fig. 7b), all thin films obtained are homogeneous for the different applied potentials, except for the presence of some cracks when the deposition potential is increased. Thus, based on the XRD, Raman, and SEM results, we can suggest that the best deposition potential for FTO is obtained between -1 and -1.1 V, with a very intense preferential peak (111) and complete homogeneity. These results agree with those obtained by Mandal et al. for SnSe on FTO obtained by electrochemical deposition [52].

The EDS spectra of the two samples presented in Fig. 8 confirm the presence of Sn and Se. Other peaks such as Si, O, N, and Cl appeared in the EDS spectrum of SnSe (Fig. 8a, b) due to the composition of the ITO and FTO substrates and the electrolyte composition. The absence of other peaks reveals the purity of the materials.

Optical analysis

The band gap energy of a semiconductor is the amount of energy required to excite an electron from the valence band to the conduction band. We used the UV–Vis diffuse reflectance

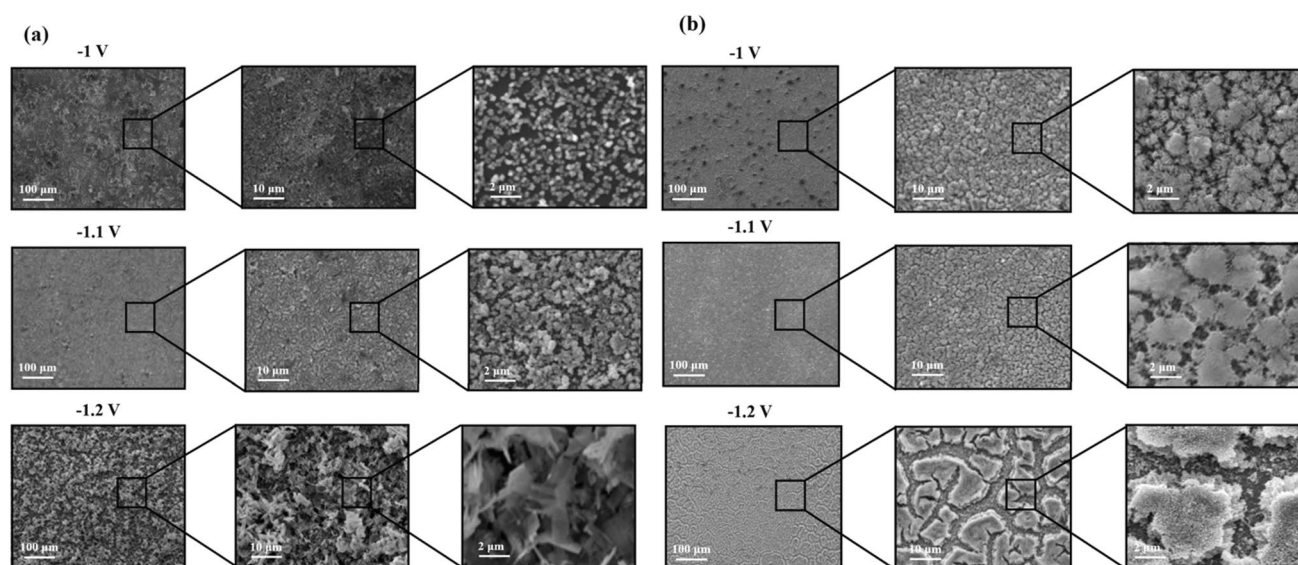
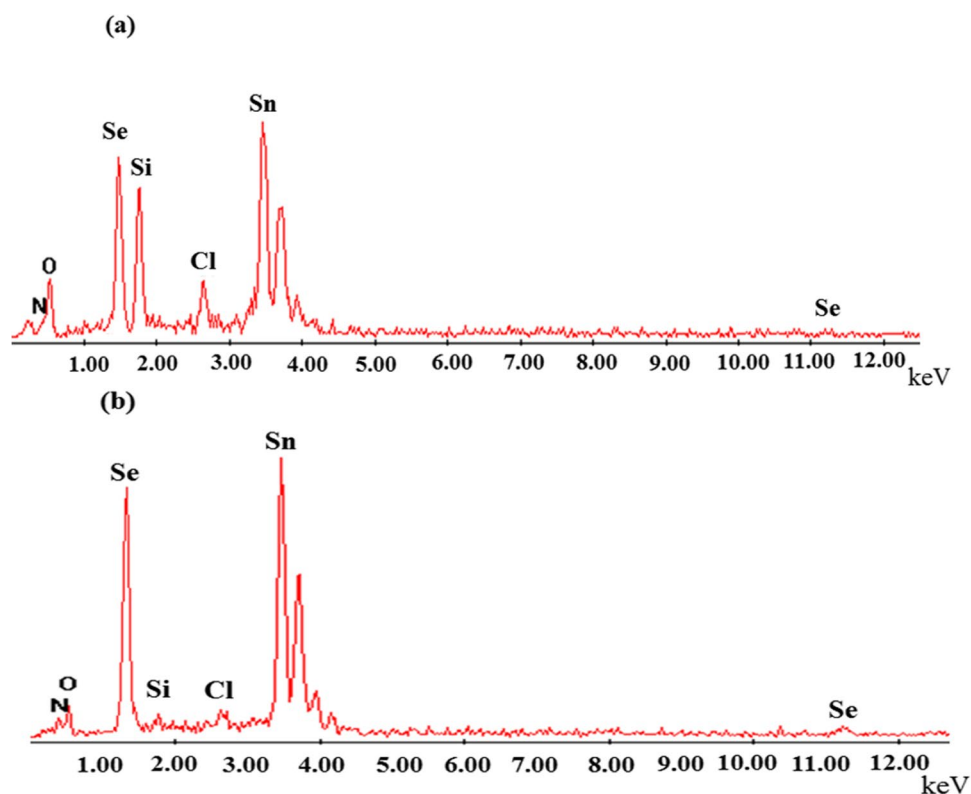


Fig. 7 SEM images of SnSe film obtained by electrodeposition at different potentials on (a) ITO and (b) FTO

Fig. 8 EDS spectra of SnSe film on (a) ITO/−1.1 V and (b) FTO/−1 V



spectrum to determine the optical characteristics and band gaps of the synthesized layers. Figure 9 shows the reflectance spectra of the samples prepared on ITO and FTO at different potentials. As shown in Fig. 9a, b, the reflectance of the SnSe layer deposited at −1.1 V is higher than that of the layer deposited at −1 V, which is higher than that of the sample

at −1.2 V. The trend of the absorption spectra can be directly related to the thickness of the SnSe layers. Using the Tauc formula [53, 54]:

$$\alpha h\nu = A(h\nu - E_g)^{1/n} \quad (13)$$

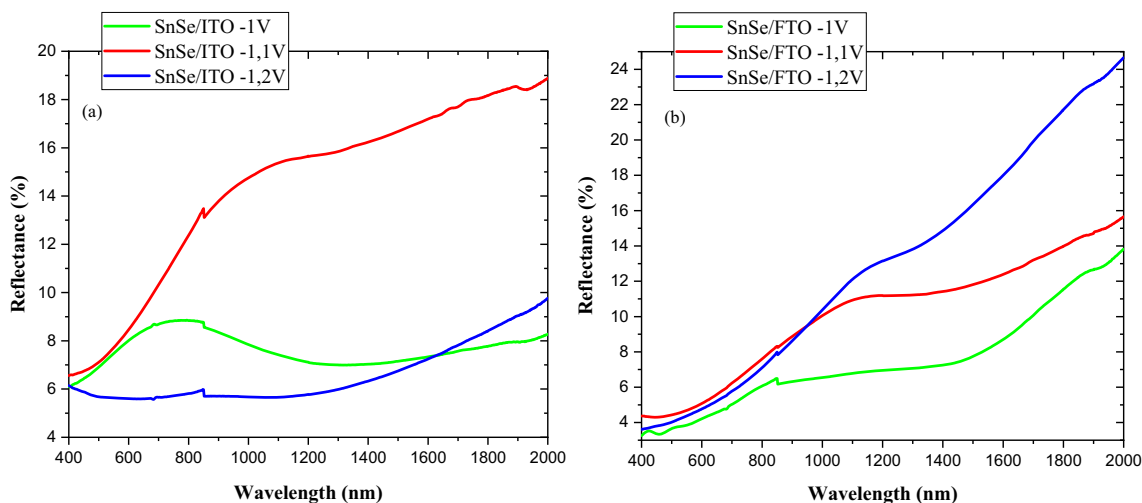


Fig. 9 Optical reflection spectrum for SnSe films deposited at -1 V, -1.1 V, and -1.2 V on (a) ITO and (b) FTO

where h is the Planck constant, ν is the frequency of photons, E_g is the energy of the band gap, A is an energy-independent constant, and n is equal to 0.5 for direct bandgap semiconductors. The energy of the band gap is typically calculated from diffuse reflectance spectra. According to the theory of P. Kubelka and F. Munk [55, 56], reflectance spectra can be converted to corresponding absorption spectra by applying the Kubelka–Munk function ($F(R_\infty)$).

$$F(R_\infty) = \frac{K}{S} = \frac{(1 - R_\infty)^2}{2R_\infty} \tag{14}$$

where $R_\infty = \frac{R_{\text{sample}}}{R_{\text{standard}}}$ is the reflectance of an infinitely thick sample, while the absorption and scattering coefficients are

represented by K and S , respectively. Putting $F(R_\infty)$ in place of α in Eq. (13) gives the following formula (15):

$$(F(R_\infty) \cdot h\nu) = A(h\nu - E_g)^{1/n} \tag{15}$$

Figure 9a, b shows the reflectance spectrum of SnSe prepared with potentials ranging from -1 to -1.2 V on ITO and FTO, transformed according to Eq. (13) and plotted as a function of photon energy, to yield the Tauc plot illustrated in Fig. 10.

The direct band gaps at potentials of -1 V, -1.1 V, and -1.2 V were calculated to be 1.71 eV, 1.25 eV, and 2.24 eV for the SnSe thin film on ITO and 2.87 eV, 1.46 eV, and 2.41 eV, respectively, for the SnSe thin film on FTO.

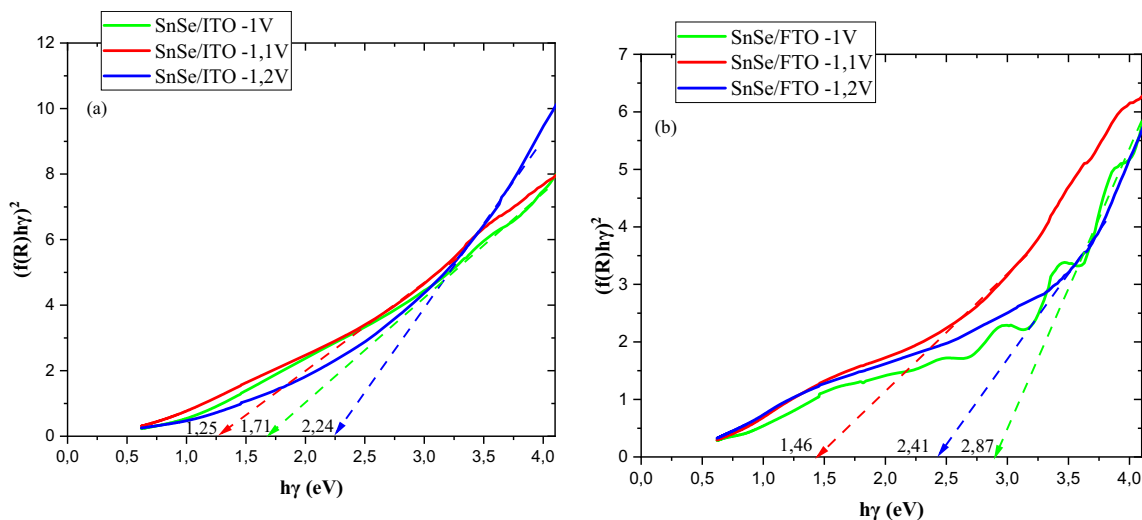


Fig. 10 Plot of Tauc $(\alpha h\nu)^2$ versus photon energy ($h\nu$) for SnSe films deposited at -1 V, -1.1 V, and -1.2 V on (a) ITO and (b) FTO

Table 1 Comparative analysis of reported band gaps for SnSe

Ref	E_g (SnSe) eV	
	ITO	FTO
[38]	1.44	
[39]	0.96–1.26	
[40]	1.05	
[26]	-	1.44
[36]	-	1
[37]	-	1.43
Our work	1.25	1.46

Compared to the various band gaps that have been reported for SnSe in previous studies (Table 1), the band gap values obtained in this study fall within the range of literature data. The band gaps are significantly different between SnSe grown on ITO and FTO because the band gaps of semiconductors are largely dependent on nanoparticle size, nanostructure, and substrate nature.

Furthermore, the Tauc plots (Fig. 10a) recorded for the SnSe thin film prepared on ITO substrate exhibit a lower band gap energy value, which can be attributed to the morphological properties of the crystal size of the SnSe/ITO sample, as illustrated by the SEM study (Fig. 7a) at -1.1 V, since larger crystal clusters increase the possibility of light scattering in the depletion regions of the respective film, thus increasing light absorption in the cell [57]. Nonetheless, the growth of these larger crystals also results in a substantial extension of the light path within the photoanode, thus facilitating the absorption of a greater number of photons by the thin layers of SnSe.

Based on the results obtained from XRD, Raman spectroscopy, SEM, and UV–vis diffuse reflectance spectra, the bandgap of the SnSe films deposited on the ITO substrate at a potential of -1.1 V makes them suitable for photovoltaic application compared to other samples deposited on FTO substrate.

Conclusions

In conclusion, this study successfully utilized a new organophosphorus compound as a selenium precursor for the electrodeposition of SnSe thin films on ITO and FTO glass substrates at room temperature. The investigation focused on the structural, morphological, and optical properties of the deposited films. The results revealed that both the substrate type and deposition potential had a significant impact on the properties of the films. The production of the SnSe phase with some presence of the SnO_2 phase was verified by XRD analysis, with the substrate type impacting the rate of phase appearance. For all the produced SnSe films, the XRD diffraction pattern revealed an orthorhombic structure with a

preferred orientation (111), and the estimated crystallite size showed the maximum values at -1.1 V for ITO and -1 V for FTO. Raman spectroscopy results supported the findings from XRD analysis. The structural and optical properties were strongly influenced by the substrate type and deposition potential. The obtained films exhibited a direct allowed transition with band gaps of 1.25 eV and 1.46 eV at -1.1 V for ITO and FTO, respectively. The optical properties suggested the potential suitability of the films for photovoltaic applications due to their low band gap. The findings indicate that SnSe films deposited on ITO at a potential of -1.1 V may exhibit enhanced sensitivity for photovoltaic structures.

Acknowledgements The authors want to acknowledge the University of Tunis El Manar for the “Alternance Bourse” granted.

Author contribution Amira Benhjal: conceptualization, methodology, formal analysis, data curation, investigation, writing – original draft, visualization. Luca Pezzato: formal analysis, investigation, data curation, writing – original draft, writing – review and editing. Elena Colusso: formal analysis, investigation, data curation, writing – original draft, writing – review and editing. Khaled ALOUANI: methodology, supervision, funding acquisition, project administration. Manuele Dabalà: conceptualization, resources, writing – review and editing, supervision, project administration, funding acquisition.

Funding Open access funding provided by Università degli Studi di Padova

Data availability The raw data of the present study will be available on request.

Declarations

Ethical approval Not applicable.

Competing interests The authors declare no competing interests.

Open Access This article is licensed under a Creative Commons Attribution 4.0 International License, which permits use, sharing, adaptation, distribution and reproduction in any medium or format, as long as you give appropriate credit to the original author(s) and the source, provide a link to the Creative Commons licence, and indicate if changes were made. The images or other third party material in this article are included in the article’s Creative Commons licence, unless indicated otherwise in a credit line to the material. If material is not included in the article’s Creative Commons licence and your intended use is not permitted by statutory regulation or exceeds the permitted use, you will need to obtain permission directly from the copyright holder. To view a copy of this licence, visit <http://creativecommons.org/licenses/by/4.0/>.

References

1. Kafashan H, Azizieh M, Balak Z (2017) Electrochemical synthesis of nanostructured Se-doped SnS: effect of Se-dopant on surface characterizations. *Appl Surf Sci* 410:186–195. <https://doi.org/10.1016/j.apsusc.2017.03.062>
2. Bouich A, Cerutti J, Chfi H, Marí-guaita J, Hameed Y, Baig F (2023) Delafossite as hole transport layer a new pathway for

- efficient perovskite-based solar cells : insight from experimental. DFT Numer Anal 250:18–32. <https://doi.org/10.1016/j.solener.2022.12.022>
3. Bouich A, Marí-guaita J (2023) Bright future by enhancing the stability of methylammonium lead triiodide perovskites thin films through Rb, Cs and Li as dopants. 163:1–10. <https://doi.org/10.1016/j.materresbull.2023.112213>
 4. Bouich A, Cerutti J, Hameed Y, Baig F, Marí-guaita J, Mendez-blas A, Palacios P (2023) Bright future by controlling α / δ phase junction of formamidinium lead iodide doped by imidazolium for solar cells : insight from experimental, DFT calculations and SCAPS simulation, 40. <https://doi.org/10.1016/j.surf.2023.103159>
 5. Jeong G, Kim J, Gunawan O, Pae SR, Kim SH, Song JY, Lee YS, Shin B (2017) Preparation of single-phase SnSe thin-films and modification of electrical properties via stoichiometry control for photovoltaic application. J Alloy Compd 722:474–481. <https://doi.org/10.1016/j.jallcom.2017.06.094>
 6. Ceylan A (2017) Synthesis of SnS thin films via high vacuum sulfidation of sputtered Sn thin films. Mater Lett 201:194–197. <https://doi.org/10.1016/j.matlet.2017.05.022>
 7. Jamali-Sheini F, Cheraghizade M, Yousefi R (2018) Electrochemically synthesis and optoelectronic properties of Pb- and Zn-doped nanostructured SnSe films. Appl Surf Sci 443:345–353. <https://doi.org/10.1016/j.apsusc.2018.03.011>
 8. Kafashan H, Azizieh M, NasiriVatan H (2016) Ultrasound-assisted electrodeposition of SnS: effect of ultrasound waves on the physical properties of nanostructured SnS thin films. J Alloys Compd 686:962–968. <https://doi.org/10.1016/j.jallcom.2016.06.201>
 9. Turan E, Kul M, Aybek AS, Zor M (2009) Structural and optical properties of SnS semiconductor films produced by chemical bath deposition. J Phys D Appl Phys 42. <https://doi.org/10.1088/0022-3727/42/24/245408>
 10. Noguchi H, Setiyadi A, Tanamura H, Nagatomo T, Omoto O (1994) Characterization of vacuum-evaporated tin sulfide film for solar cell materials. Sol Energy Mater Sol Cells 35:325–331. [https://doi.org/10.1016/0927-0248\(94\)90158-9](https://doi.org/10.1016/0927-0248(94)90158-9)
 11. Price LS, Parkin IP, Hardy AME, Clark RJH, Hibbert TG, Mollroy KC (1999) Atmospheric pressure chemical vapor deposition of tin sulfides (SnS, Sn₂S₃, and SnS₂) on glass. Chem Mater 11:1792–1799. <https://doi.org/10.1021/cm990005z>
 12. Ogah OE, Reddy KR, Zoppi G, Forbes I, Miles RW (2011) Annealing studies and electrical properties of SnS-based solar cells. Thin Solid Films 519:7425–7428. <https://doi.org/10.1016/j.tsf.2010.12.235>
 13. Zhu H, Yang D, Ji Y, Zhang H, Shen X (2005) Two-dimensional SnS nanosheets fabricated by a novel hydrothermal method. J Mater Sci 40:591–595. <https://doi.org/10.1007/s10853-005-6293-x>
 14. Hartman K, Johnson JL, Bertoni MI, Recht D, Aziz MJ, Scarpulla MA, Buonassisi T (2011) SnS thin-films by RF sputtering at room temperature. Thin Solid Films 519:7421–7424. <https://doi.org/10.1016/j.tsf.2010.12.186>
 15. Ghosh B, Das M, Banerjee P, Das S (2008) Fabrication and optical properties of SnS thin films by SILAR method. Appl Surf Sci 254:6436–6440. <https://doi.org/10.1016/j.apsusc.2008.04.008>
 16. Teghil R, Santagata A, Marotta V, Orlando S, Pizzella G, Giardini-Guidoni A, Mele A (1995) Characterization of the plasma plume and of thin film epitaxially produced during laser ablation of SnSe. Appl Surf Sci 90:505–514. [https://doi.org/10.1016/0169-4332\(95\)00179-4](https://doi.org/10.1016/0169-4332(95)00179-4)
 17. Gregory BW, Stickney JL (1991) Electrochemical atomic layer epitaxy (ECALE). J Electroanal Chem 300:543–561. [https://doi.org/10.1016/0022-0728\(91\)85415-L](https://doi.org/10.1016/0022-0728(91)85415-L)
 18. Burton MR, Boyle CA, Liu T, McGettrick J, Nandhakumar I, Fenwick O, Carnie MJ (2020) Full thermoelectric characterization of stoichiometric electrodeposited thin film tin selenide (SnSe). ACS Appl Mater Interfaces 12:28232–28238. <https://doi.org/10.1021/acsami.0c06026>
 19. Manivannan R, Victoria SN (2018) Preparation of chalcogenide thin films using electrodeposition method for solar cell applications – a review. Sol Energy 173:1144–1157. <https://doi.org/10.1016/j.solener.2018.08.057>
 20. Jeffrey CA, Harrington DA, Morin S (2002) In situ scanning tunneling microscopy of bismuth electrodeposition on Au(1 1 1) surfaces. Surf Sci 512:5–10. [https://doi.org/10.1016/S0039-6028\(02\)01685-0](https://doi.org/10.1016/S0039-6028(02)01685-0)
 21. Zhou X, Gan L, Tian W, Zhang Q, Jin S, Li H, Bando Y, Golberg D, Zhai T (2015) Ultrathin SnSe₂ flakes grown by chemical vapor deposition for high-performance photodetectors. Adv Mater 27:8035–8041. <https://doi.org/10.1002/adma.201503873>
 22. Fan Y, Yang J, Jiang L, Wang Y, Ng BK, Sun H, Lai Y, Li J, Liu F (2017) Effects of illumination on the electrochemical behavior of selenium electrodeposition on ITO substrates. J Electrochem Soc 164:H225–H231. <https://doi.org/10.1149/2.1481704jes>
 23. Han W, Cao LY, Huang JF, Wu JP (2009) Influence of pH value on PbS thin films prepared by electrodeposition. Mater Technol 24:217–220. <https://doi.org/10.1179/175355509X447195>
 24. Zhu W, Liu X, Liu H, Tong D, Yang J, Peng J (2010) Coaxial heterogeneous structure of TiO₂ nanotube arrays with CdS as a superthin coating synthesized via modified electrochemical atomic layer deposition. J Am Chem Soc 132:12619–12626. <https://doi.org/10.1021/ja102511z>
 25. Köse H, Biçer M, Tütünoğlu Ç, Aydın AO, Şişman I (2009) The underpotential deposition of Bi₂Te₃-ySe_y thin films by an electrochemical co-deposition method. Electrochim Acta 54:1680–1686. <https://doi.org/10.1016/j.electacta.2008.09.059>
 26. Biçer M, Aydın AO, Şişman I (2010) Electrochemical synthesis of CdS nanowires by underpotential deposition in anodic alumina membrane templates. Electrochim Acta 55:3749–3755. <https://doi.org/10.1016/j.electacta.2010.02.015>
 27. Biçer M, Köse H, Şişman I (2010) Selective electrodeposition and growth mechanism of thermoelectric bismuth-based binary and ternary thin films. J Phys Chem C 114:8256–8263. <https://doi.org/10.1021/jp101221u>
 28. Doumbia Y, Bouich A, Soro D (2022) Optik Mixed halide head perovskites thin films : stability and growth investigation. 261:1–7. <https://doi.org/10.1016/j.ijleo.2022.169222>
 29. Gao W, Li Y, Guo J, Ni M, Liao M, Mo H, Li J (2018) Narrow-gap physical vapour deposition synthesis of ultrathin SnS_{1-x}: XSex (0 ≤ x ≤ 1) two-dimensional alloys with unique polarized Raman spectra and high (opto)electronic properties. Nanoscale 10:8787–8795. <https://doi.org/10.1039/c8nr00856f>
 30. Benjamin SL, De Groot CHK, Gurnani C, Hawken SL, Hector AL, Huang R, Jura M, Levason W (2018) <https://doi.org/10.1039/C8TC01285G>, 7734–7739. <https://doi.org/10.1039/c8tc01285g>
 31. Assili K, Gonzalez O, Alouani K, Vilanova X (2017) Structural, morphological, optical and sensing properties of SnSe and SnSe₂ thin films as a gas sensing material. Arab J Chem. <https://doi.org/10.1016/j.arabjc.2017.10.004>
 32. Assili K, Alouani K, Vilanova X (2017) Structural and optical properties of tin (II) sulfide thin films deposited using organophosphorus precursor (Ph₃PS). Semicond Sci Technol 32. <https://doi.org/10.1088/1361-6641/32/2/025002>
 33. Zainal Z, Ali AJ, Kassim A, Hussein MZ (2003) Electrodeposition of tin selenide thin film semiconductor: effect of the electrolytes concentration on the film properties. Sol Energy Mater Sol Cells 79:125–132. [https://doi.org/10.1016/S0927-0248\(02\)00392-6](https://doi.org/10.1016/S0927-0248(02)00392-6)
 34. Subramanian B, Mahalingam T, Sanjeeviraja C, Jayachandran M, Chockalingam MJ (1999) Electrodeposition of Sn, Se, SnSe and

- the material properties of SnSe films. *Thin Solid Films* 357:119–124. [https://doi.org/10.1016/S0040-6090\(99\)00644-6](https://doi.org/10.1016/S0040-6090(99)00644-6)
35. Ju H, Park D, Kim J (2017) Hydrothermal transformation of SnSe crystal to Se nanorods in oxalic acid solution and the outstanding thermoelectric power factor of Se/SnSe composite. *Sci Rep* 7:1–6. <https://doi.org/10.1038/s41598-017-18508-2>
 36. Mao BW, Tang J, Randler R (2002) Clustering and anisotropy in monolayer formation under potential control: Sn on Au(111). *Langmuir* 18:5329–5332. <https://doi.org/10.1021/la011327w>
 37. Massaccesi S, Sanchez S, Vedel J (1996) Electrodeposition of indium selenide In₂Se₃. *J Electroanal Chem* 412:95–101. [https://doi.org/10.1016/0022-0728\(96\)04604-9](https://doi.org/10.1016/0022-0728(96)04604-9)
 38. Mishra KK, Rajeshwar K (1989) A voltammetric study of the electrodeposition chemistry in the Cu + In + Se system. *J Electroanal Chem* 271:279–294. [https://doi.org/10.1016/0022-0728\(89\)80082-8](https://doi.org/10.1016/0022-0728(89)80082-8)
 39. Dilmi O, Benaicha M, Asseli R (2021) Electroplating kinetic of nanostructured selenium films from citrate bath. *Chem Africa* 4:85–93. <https://doi.org/10.1007/s42250-020-00209-5>
 40. Jarzabek C, Kublik Z (1980) Cyclic and stripping voltammetry of Se(+4) and Se(-2) AT carbon electrodes in acid solutions. *J Electroanal Chem* 21:1389–1392. [https://doi.org/10.1016/S0022-0728\(80\)80445-1](https://doi.org/10.1016/S0022-0728(80)80445-1)
 41. Qiao Z, Shang W, Wang C (2005) Fabrication of Sn-Se compounds on a gold electrode by electrochemical atomic layer epitaxy. *J Electroanal Chem* 576:171–175. <https://doi.org/10.1016/j.jelechem.2004.10.015>
 42. Shi X, Zhang X, Tian Y, Shen C, Wang C, Gao HJ (2012) Electrodeposition of Sb₂Se₃ on indium-doped tin oxides substrate: nucleation and growth. *Appl Surf Sci* 258:2169–2173. <https://doi.org/10.1016/j.apsusc.2011.02.097>
 43. Ham S, Choi S, Chae Y, Lee WJ, Paeng KJ, Kim WG, Myung N (2010) Photoelectrochemical deposition of SnSe thin films on a Se-modified polycrystalline gold substrate. *Bull Korean Chem Soc* 31:3403–3406. <https://doi.org/10.5012/bkcs.2010.31.11.3403>
 44. Mathews NR (2012) Electrodeposited tin selenide thin films for photovoltaic applications. *Sol Energy* 86:1010–1016. <https://doi.org/10.1016/j.solener.2011.06.012>
 45. Khan MD, Aamir M, Sohail M, Sher M, Baig N, Akhtar J, Malik MA, Revaprasadu N (2018) Bis(selenobenzoato)dibutyltin(IV) as a single source precursor for the synthesis of SnSe nanosheets and their photo-electrochemical study for water splitting. *Dalton Trans* 47:5465–5473. <https://doi.org/10.1039/c8dt00285a>
 46. Li XZ, Xia J, Wang L, Gu YY, Cheng HQ, Meng XM (2017) Layered SnSe nano-plates with excellent in-plane anisotropic properties of Raman spectrum and photo-response. *Nanoscale* 9:14558–14564. <https://doi.org/10.1039/c7nr05047j>
 47. Fernandes PA, Sousa MG, Salomé PMP, Leitão JP, Da Cunha AF (2013) Thermodynamic pathway for the formation of SnSe and SnSe₂ polycrystalline thin films by selenization of metal precursors. *CrystEngComm* 15:10278–10286. <https://doi.org/10.1039/c3ce41537f>
 48. Zhang J, Peng Z, Soni A, Zhao Y, Xiong Y, Peng B, Wang J, Dresselhaus MS, Xiong Q (2011) Raman spectroscopy of few-quintuple layer topological insulator Bi₂Se₃ nanoplatelets. *Nano Lett* 11:2407–2414. <https://doi.org/10.1021/nl200773n>
 49. Anwar S, Gowthamaraju S, Mishra BK, Singh SK, Anwar S (2015) Spray pyrolysis deposited tin selenide thin films for thermoelectric applications. *Mater Chem Phys* 1–7. <https://doi.org/10.1016/j.matchemphys.2015.01.008>
 50. Dhanasekaran V, Jung J, Lee KK, Mahalingam T (2015) Comparison studies on electrodeposited CdSe, SnSe and Cd_xSn_{1-x}Se thin films. *Ionics* 21:1187–1192. <https://doi.org/10.1007/s11581-014-1251-8>
 51. Shinde DV, Min SK, Sung MM, Shrestha NK, Mane RS, Han SH (2014) Photovoltaic properties of nanocrystalline SnSe–CdS. *Mater Lett* 115:244–247. <https://doi.org/10.1016/j.matlet.2013.10.073>
 52. Mandal P, Show B, Ahmed ST, Banerjee D, Mondal A (2020) Visible-light active electrochemically deposited tin selenide thin films: synthesis, characterization and photocatalytic activity. *J Mater Sci Mater Electron* 31:4708–4718. <https://doi.org/10.1007/s10854-020-03027-0>
 53. Abrari M, Ahmadi M, Ghanaatshoar M, Moazami HR, Davarani SSH (2019) Fabrication of dye-sensitized solar cells based on SnO₂/ZnO composite nanostructures: a new facile method using dual anodic dissolution. *J Alloy Compd* 784:1036–1046. <https://doi.org/10.1016/j.jallcom.2018.12.299>
 54. Makula P, Pacia M, Macyk W (2018) How to correctly determine the band gap energy of modified semiconductor photocatalysts based on UV-Vis spectra. *J Phys Chem Lett* 9:6814–6817. <https://doi.org/10.1021/acs.jpcclett.8b02892>
 55. Vaughn DD, II In S, Schaak RE (2011) A precursor-limited nanoparticle coalescence pathway for tuning the thickness of laterally-uniform colloidal nanosheets: the case of SnSe. *ACS Nano* 5:8852–8860. <https://doi.org/10.1021/nn203009v>
 56. Jalalian-Larki B, Jamali-Sheini F, Yousefi R (2020) Electrodeposition of in-doped SnSe nanoparticles: correlation of physical characteristics with solar cell performance. *Solid State Sci* 108:106388. <https://doi.org/10.1016/j.solidstatesciences.2020.106388>
 57. Patel K, Solanki G, Patel K, Pathak V, Chauhan P (2019) Investigation of optical, electrical and optoelectronic properties of SnSe crystals. *Eur Phys J B* 92. <https://doi.org/10.1140/epjb/e2019-100306-8>

Publisher's Note Springer Nature remains neutral with regard to jurisdictional claims in published maps and institutional affiliations.